



Published in final edited form as:

*J Am Chem Soc.* 2011 September 7; 133(35): 13967–13974. doi:10.1021/ja203756x.

## Intermolecular structure determination of amyloid fibrils with magic-angle spinning and dynamic nuclear polarization NMR

Marvin J. Bayro<sup>1</sup>, Galia T. Debelouchina<sup>1</sup>, Matthew T. Eddy<sup>1</sup>, Neil R. Birkett<sup>2,†</sup>, Catherine E. MacPhee<sup>2</sup>, Melanie Rosay<sup>3</sup>, Werner E. Maas<sup>3</sup>, Christopher M. Dobson<sup>2</sup>, and Robert G. Griffin<sup>1</sup>

Robert G. Griffin: rgg@mit.edu

<sup>1</sup>Francis Bitter Magnet Laboratory and Department of Chemistry Massachusetts Institute of Technology, Cambridge, MA 02139 USA

<sup>2</sup>Department of Chemistry, University of Cambridge, Cambridge CB2 1EW, United Kingdom

<sup>3</sup>Bruker BioSpin Corporation, Billerica, MA 01821, USA

### Abstract

We describe magic-angle spinning NMR experiments designed to elucidate the interstrand architecture of amyloid fibrils. Three methods are introduced for this purpose, two being based on the analysis of long-range <sup>13</sup>C-<sup>13</sup>C correlation spectra and a third based on the identification of intermolecular interactions in <sup>13</sup>C-<sup>15</sup>N spectra. We show, in studies of fibrils formed by the 86-residue SH3 domain of PI3 kinase (PI3-SH3), that efficient <sup>13</sup>C-<sup>13</sup>C correlation spectra display a resonance degeneracy that establishes a parallel, in-register alignment of the proteins in the amyloid fibrils. In addition, this degeneracy can be circumvented to yield direct intermolecular constraints. The <sup>13</sup>C-<sup>13</sup>C experiments are corroborated by <sup>15</sup>N-<sup>13</sup>C correlation spectrum obtained from a mixed [<sup>15</sup>N, <sup>12</sup>C]/[<sup>14</sup>N, <sup>13</sup>C] sample which directly quantifies interstrand distances. Furthermore, when the spectra are recorded with signal enhancement provided by dynamic nuclear polarization (DNP) at 100 K, we demonstrate a dramatic increase (from 23 to 52) in the number of intermolecular <sup>15</sup>N-<sup>13</sup>C constraints present in the spectra. The increase in the information content is due to the enhanced signal intensities and to the fact that dynamic processes, leading to spectral intensity losses, are quenched at low temperatures. Thus, acquisition of low temperature spectra addresses a problem that is frequently encountered in MAS spectra of proteins. In total the experiments provide 111 intermolecular <sup>13</sup>C-<sup>13</sup>C and <sup>15</sup>N-<sup>13</sup>C constraints that establish that the PI3-SH3 protein strands are aligned in a parallel, in-register arrangement within the amyloid fibril.

### Keywords

Amyloid fibrils; magic angle spinning; dynamic nuclear polarization; phosphatidylinositol-3-kinase SH3 domain (PI3-SH3)

Amyloid fibrils are high molecular weight aggregates formed by peptides and proteins with a characteristic cross- $\beta$  structure in which  $\beta$ -sheets run parallel to the fibril axis.<sup>1-3</sup> A wide range of debilitating pathologies, including neurodegenerative disorders such as Alzheimer's disease and other conditions such as type 2 diabetes, involve amyloid fibrils and/or their precursor aggregates.<sup>4</sup> In addition, non-pathological and functional amyloid assemblies have been recognized,<sup>5</sup> and the observation of fibril formation by peptides and proteins unrelated

Correspondence to: Robert G. Griffin, rgg@mit.edu.

<sup>†</sup>Present addresses: MedImmune, Milstein Building, Granta Park, Cambridge, CB21 6GH, UK

to disease indicates that the amyloid fold is a generally accessible state of polypeptide chains.<sup>3, 4, 6</sup> There is therefore a very significant interest in deciphering the molecular architecture of amyloid fibrils and their precursors, from both the biomedical and the fundamental biophysical perspectives.

The structures of proteins in amyloid fibrils differ conceptually from those of natively folded monomers. While the tertiary structure of monomers is the result of intramolecular forces, the structure in fibrils is typically determined by intermolecular interactions that give rise to the core  $\beta$ -sheet assembly.<sup>7</sup> In principle, the  $\beta$ -sheets in amyloid fibrils can be formed by parallel or antiparallel  $\beta$ -strands, or a combination of both, and with residues in or out of register between neighboring molecules.<sup>8, 9</sup> The overall topology of amyloid fibrils is then defined by the relative positions and orientations of the  $\beta$ -sheets that compose the core of the fibril.

Despite the complexity of the molecular design of these structures, magic-angle spinning nuclear magnetic resonance (MAS NMR) studies have resulted in the elucidation of structural information relating to amyloid fibrils at the secondary structure level via resonance assignment and chemical shift analysis<sup>10-16</sup> and precise distance and torsion angle measurements.<sup>17</sup> In addition, approximate distance constraints have been used to propose models for various systems.<sup>18-22</sup> In the case of amyloid fibrils formed by peptides amenable to solid-phase synthesis, the tertiary structure can be probed by the incorporation of  $^{13}\text{C}$  or  $^{15}\text{N}$  labels at specific residues. A possible motif is a parallel, in-register arrangement of the  $\beta$ -sheets, which can be tested by incorporation of a single  $^{13}\text{C}$  label in all the molecules and the measurement of  $^{13}\text{C}$ - $^{13}\text{C}$  dipolar couplings.<sup>8</sup> These measurements are typically performed for various residues along the sequence using separate samples and in one-dimensional (1D) fashion. Several studies have utilized this and similar approaches, such as inserting pairs of  $^{13}\text{C}/^{13}\text{C}$  or  $^{13}\text{C}/^{15}\text{N}$  nuclei, to derive models of the interstrand structure of fibrils formed by peptides.<sup>8, 23-27</sup>

However, specific labeling in biosynthetically produced proteins relies on incorporating singly  $^{13}\text{C}$ -labeled amino acids in the growth medium, resulting in the labeling of all positions of a given amino acid type throughout the sequence and thus compromising the resolution. Although such an approach can reveal structural information,<sup>20, 21</sup> methods that yield data for multiple resolved sites are more general and advantageous in structural studies of protein fibrils. An example of a multiple-site approach is that involving the preparation of fibrils with a mixture of [ $^{13}\text{C}$ ,  $^{14}\text{N}$ ] and [ $^{12}\text{C}$ ,  $^{15}\text{N}$ ] labeled molecules and obtaining  $^{15}\text{N}$ - $^{13}\text{C}$  constraints between adjacent molecules in 2D heteronuclear correlation spectra. This mixed-sample approach has been previously applied to protein fibrils,<sup>22</sup> and is enhanced by sparse  $^{13}\text{C}$  labeling.<sup>28, 29</sup> Nevertheless, such heteronuclear experiments typically suffer from inherently low sensitivity, which is aggravated by spin dilution and the long internuclear distances involved. As a result they have not been widely applicable.

Here we describe three experimental approaches directed towards the determination of the intermolecular tertiary structure of amyloid fibrils via MAS NMR spectroscopy and demonstrate their application to fibrils formed by the SH3 domain of PI3 kinase (PI3-SH3), an 86-residue protein that has been thoroughly characterized as a model for fibril formation.<sup>30-33</sup> We show that the examination of long-range  $^{13}\text{C}$ - $^{13}\text{C}$  correlation spectra of samples prepared with alternating  $^{13}\text{C}$ - $^{12}\text{C}$  labeling<sup>34, 35</sup> leads to the detection of indirect and direct intermolecular constraints for multiple sites along the polypeptide chain. These homonuclear approaches are validated with heteronuclear experiments in a mixed  $^{15}\text{N}/^{13}\text{C}$  sample. In addition, we demonstrate that dynamic nuclear polarization (DNP) -enhanced MAS NMR experiments performed at 100 K yield spectra with excellent signal-to-noise ratios and sufficient resolution to observe intermolecular heteronuclear correlations in mixed

samples, confirming a parallel, in-register structure in PI3-SH3 amyloid fibrils. Importantly, this study illustrates a situation where a cryoprotected sample enables spectra to be recorded at low temperatures, and validates a powerful, versatile approach for the investigation of supramolecular interactions in protein assemblies and complexes.

## Results and discussion

### $^{13}\text{C}$ - $^{13}\text{C}$ correlations between $\beta$ -strands

Homonuclear  $^{13}\text{C}$ - $^{13}\text{C}$  correlations between distant nuclei may in principle yield the information necessary to identify intermolecular interactions, provided that such correlations can be measured with sufficient sensitivity and resolution. The band-selective radio frequency-driven recoupling (BASE RFDR) scheme, in combination with alternating  $^{13}\text{C}$ - $^{12}\text{C}$  labeling (achieved through the use of  $[2\text{-}^{13}\text{C}]$  glycerol in the growth medium), efficiently generates cross-peaks in correlation spectra between aliphatic  $^{13}\text{C}$  nuclei such as  $^{13}\text{C}\alpha(i)$ - $^{13}\text{C}\alpha(i\pm 1)$  and  $^{13}\text{C}\alpha(i)$ - $^{13}\text{C}\beta(i\pm 1)$ .<sup>36</sup> Multiple factors contribute to the efficiency of this approach, including (1) the robust character of RFDR-type pulse sequences with respect to experimental imperfections,<sup>37, 38</sup> (2) the absence of heteronuclear interference because the low  $^{13}\text{C}$  power levels avoid depolarization processes, (3) the favorable recoupling effect of finite pulses, (4) the narrow effective recoupling bandwidth, restricted to the aliphatic region of the spectrum, that eliminates unwanted  $^{13}\text{C}\alpha(i)$ - $^{13}\text{C}'(i-1)$  polarization transfer, and (5) the attenuation of dipolar truncation effects afforded by sparse  $^{13}\text{C}$  labeling.<sup>39</sup>

In order to establish the validity of this approach, we recorded BASE RFDR spectra of a microcrystalline sample of protein  $\text{G}_{\text{B}1}$  prepared with  $[2\text{-}^{13}\text{C}]$  glycerol ( $2\text{-G}_{\text{B}1}$ ). The spectra exhibit cross-peaks with excellent signal intensities both between sequential residues and between residues distant in the sequence. Indeed, with mixing times  $\geq 20$  ms, long-range cross-peaks between many backbone  $^{13}\text{C}$  sites were observed, corresponding to internuclear distances of up to 6.5 Å. As a representative example, the strip plot of Fig. 1a shows cross-peaks between  $\text{Y45C}\alpha$  and  $\text{C}\alpha$  nuclei from residues T44, D46, D47, T51, F52, K13, and G14. Fig. 1b illustrates the environment surrounding  $\text{Y45C}\alpha$ , which includes part of a neighboring protein molecule in the crystal lattice. Residue Y45 is located in one of the outer  $\beta$ -strands of  $\text{G}_{\text{B}1}$  and forms an antiparallel  $\beta$ -sheet with another strand that includes T51 and F52. In addition, Y45 is in close proximity to K13 and G14, which are part of a  $\beta$ -strand in an adjacent molecule and are denoted with asterisks in Fig. 1. Therefore, several of the backbone-backbone BASE RFDR correlations of  $\text{Y45C}\alpha$  correspond to interactions between adjacent  $\beta$ -strands, both within the molecule and across neighboring molecules. The  $\text{Y45-D47}$  cross-peak corresponds to an internuclear distance of 6.2 Å, which is greater than most interstrand correlations, and is an example of a contact that is distant in space but not in the sequence. The intensity of this ( $i$  to  $i\pm 2$ ) cross-peak is approximately three times lower than those between sequential residues and similar to those between residues in adjacent  $\beta$ -strands.

The pattern of BASE RFDR cross-peaks observed between the antiparallel  $\beta$ -strands of  $\text{G}_{\text{B}1}$  would also be expected for parallel  $\beta$ -strands, since the inter-nuclear  $^{13}\text{C}\alpha$ - $^{13}\text{C}\alpha$  distances involved are similar in both cases. Fig. 2 depicts an arrangement of three parallel  $\beta$ -strands and indicates the possible  $\text{C}\alpha$ - $\text{C}\alpha$  contacts within approximately 6.5 Å from a central residue in the middle strand. Three distinct  $\beta$ -strands ( $i$ ,  $h$ , and  $k$ ) are illustrated in Fig. 2 (left). In this case, BASE RFDR correlations are expected between residue  $i$  and other residues in all three strands ( $i\pm 1$ ,  $i\pm 2$ ;  $h$ ,  $h\pm 1$ ;  $k$ ,  $k\pm 1$ ) and would be detected in 2D spectra provided that the resonances are resolved, as they are for  $2\text{-G}_{\text{B}1}$ . However, the specific case of parallel, in-register  $\beta$ -strands, which is common in amyloid fibrils, results in complete degeneracy of cross-peaks between interstrand and intrastrand contacts. Fig. 2 (right) illustrates such in-

register formation, which consists of identical  $\beta$ -strands and yields correlation spectra in which interstrand correlations are fully overlapped with sequential correlations or the diagonal peak. We may therefore conclude that parallel, in-register structures cannot be *directly* identified (without specific labeling) in  $^{13}\text{C}$ - $^{13}\text{C}$  correlation spectra due to resonance degeneracy.

### Indirect determination of parallel, in-register tertiary structure

We proceeded to record similar spectra of PI3-SH3 amyloid fibrils produced with [ $2\text{-}^{13}\text{C}$ ] glycerol labeling (2-PI3-SH3). An important consideration was to attempt to obtain data with similar sensitivity to that achieved with 2- $G_{B1}$ . The  $^{13}\text{C}$  cross-polarization spectra of PI3-SH3 fibrils had signal-to-noise ratios approximately four times lower than those of microcrystalline  $G_{B1}$  (due to differences in the amounts of sample used, their density, and the smaller size of  $G_{B1}$ , 56 versus 86 residues); we therefore averaged BASE RFDR spectra of 2-PI3-SH3 for a period of 5 days. Long-term acquisition of 2D experiments such as BASE RFDR is feasible with minimal recalibration between consecutive runs, which allows the experiments to be recorded over several days with high fidelity.

Fig. 3 illustrates a section of a BASE RFDR spectrum of 2-PI3-SH3 acquired with a 24 ms mixing period and other parameters similar to those used for the experiment on 2- $G_{B1}$  shown in Fig. 1. Several sequential  $^{13}\text{C}\alpha$ - $^{13}\text{C}\alpha$  cross-peaks are indicated for different regions of the PI3-SH3 sequence, namely M3-S4-A5, R11-A12-L13-Y14, and F44-S45-D46. Chemical shift analysis indicates that the first two segments adopt a  $\beta$ -strand conformation while the last one is part of a well-defined loop.<sup>16</sup> Interestingly, in addition to sequential cross-peaks between adjacent residues ( $i$  to  $i\pm 1$ ) there are also cross-peaks between  $^{13}\text{C}\alpha$  nuclei separated by two residues ( $i$  to  $i\pm 2$ ), which correspond to internuclear distances of up to 6.5 Å in  $\beta$ -strand regions. The presence of such cross-peaks (labeled in black in Fig 3.) demonstrates that correlations between backbone  $^{13}\text{C}$  nuclei distant in space, as was found for 2- $G_{B1}$ , are also observed for 2-PI3-SH3 amyloid fibrils with BASE RFDR experiments. Furthermore, generation of ( $i$  to  $i\pm 2$ ) cross-peaks via dipolar recoupling suggests that the segments involved exhibit favorable dynamics, which could otherwise interfere with polarization transfer,<sup>40-43</sup> and that long-range correlations can be expected within a threshold of  $\sim 6.5$  Å in the vicinity of these residues with intensities approximately three times lower than those of sequential ( $i$  to  $i\pm 1$ )  $^{13}\text{C}\alpha$ - $^{13}\text{C}\alpha$  cross-peaks.

However, despite the detection of cross-peaks with excellent signal intensities between nuclei distant in space, no cross-peaks between  $^{13}\text{C}\alpha$  nuclei distant in sequence ( $i$  to  $i\pm 4$  or longer) can be identified for any of the multiple well-resolved sites in BASE RFDR spectra of 2-PI3-SH3 amyloid fibrils. This result is consistent with the degenerate backbone structure of a parallel, in-register intermolecular conformation discussed above. Indeed, as shown in 2- $G_{B1}$  spectra and illustrated in Fig. 2, multiple inter-strand contacts are expected for each  $^{13}\text{C}\alpha$  site in a  $\beta$ -sheet. In the case of the segments shown in Fig. 3, M3-A5 and R11-Y14 adopt a  $\beta$ -strand conformation and are expected to give rise to correlations across the component  $\beta$ -sheets while F44-D46 is part of a loop or turn and thus will not necessarily interact with distant residues. Another important caveat to consider is the possibility that the absence of correlations may be due to low fractional populations of  $^{13}\text{C}$  labeling at a given site, but that possibility can be discounted by the analysis of multiple sites along the backbone, as we found in PI3-SH3. Together with the observation of ( $i$  to  $i\pm 2$ ) correlations as local controls of efficient dipolar recoupling, the absence of correlations between backbone sites distant in sequence for  $\beta$ -strand segments implies a parallel, in-register  $\beta$ -sheet tertiary structure in PI3-SH3 amyloid fibrils.

## Direct determination of parallel, in-register tertiary structure

Alternating  $^{13}\text{C}$ - $^{12}\text{C}$  labeling results in an intercalating pattern in which certain residue types contain pairs of directly bonded sites (e.g.,  $\text{C}\alpha$ - $\text{C}\beta$ ) that are not labeled simultaneously in the same molecule, but they are each labeled independently in different molecules. Such mutually exclusive sites do not yield cross-peaks in one-bond, intraresidue  $^{13}\text{C}$ - $^{13}\text{C}$  correlation spectra. Nevertheless, long-range  $^{13}\text{C}$ - $^{13}\text{C}$  correlation spectra of 2-PI3-SH3 amyloid fibrils, recorded with extended mixing periods of BASE RFDR, proton-driven spin diffusion (PDS),<sup>44</sup> and other techniques, exhibit a number of  $^{13}\text{C}\alpha$ - $^{13}\text{C}\beta$  cross-peaks from residue types that are expected to contain mutually exclusive  $\text{C}\alpha$ - $\text{C}\beta$  labeled sites.

To identify the origin of these unexpected cross-peaks, we compared one-bond  $^{13}\text{C}$ - $^{13}\text{C}$  correlation spectra of a sample prepared with uniform  $^{13}\text{C}$  labeling (U-PI3-SH3, Fig. 4a) and 2-PI3-SH3 (Fig. 4b). These spectra demonstrate that many directly bonded  $^{13}\text{C}\alpha$ - $^{13}\text{C}\beta$  pairs in U-PI3-SH3 are indeed not labeled concurrently in 2-PI3-SH3, while others remain. Most signals that are absent in Fig. 4b correspond to residues that undergo scrambling during synthesis, such as Glu, Gln, Asp, Asn, Met, and Thr. In particular, Asp and Asn one-bond  $^{13}\text{C}\alpha$ - $^{13}\text{C}\beta$  cross-peaks vanish completely in 2-PI3-SH3, as highlighted by the dashed boxes in Fig. 4a-b. On the other hand, multiple cross-peaks are observed in this region at long mixing times, as illustrated in Fig 4c ( $\tau_{\text{PDS mix}} = 500$  ms). Similar cross-peaks are observed in long-range BASE RFDR experiments. Among the emerging cross-peaks,  $^{13}\text{C}\alpha$ - $^{13}\text{C}\beta$  correlations can be identified for residues M3, D15, D25, T33, N35, D46, N59, N62, D70, and T74, and assigned to intermolecular contacts, since they are not observed with the short mixing time that enables the identification of one-bond contacts in 2-PI3-SH3. Each of these residues in a given molecule must be in close proximity ( $<7$  Å) to the same residue in an adjacent molecule within the fibrils. Since multiple correlations are established throughout the PI3-SH3 sequence, these cross-peaks specify a parallel, in-register fibril arrangement.

The mutually exclusive fractional labeling pattern produced in some residue types by alternating labeling enables the identification of interactions between adjacent molecules forming  $\beta$ -sheets in PI3-SH3 fibrils via  $^{13}\text{C}$ - $^{13}\text{C}$  correlation experiments with long mixing periods. It is essential to ensure that the  $^{13}\text{C}\alpha$ - $^{13}\text{C}\beta$  pairs of interest are not labeled concurrently in the same molecule in order to verify the long-range character of their correlations. Thus, the examination of  $^{13}\text{C}$ - $^{13}\text{C}$  spectra of 2-PI3-SH3 with long and short mixing times leads to the direct observation of correlations between neighboring molecules and the identification of a parallel, in-register intermolecular structure within these amyloid fibrils. This direct method is conceptually similar to utilizing mixtures of differentially  $^{13}\text{C}$  labeled molecules,<sup>45</sup> although additional control samples are employed in such an approach.

## Heteronuclear correlations enhanced by dynamic nuclear polarization

To corroborate the homonuclear correlation methodology described above and to obtain additional constraints on the tertiary structure of PI3-SH3 fibrils, we prepared a fibril sample from a mixture of  $[\text{U-}^{15}\text{N}]$  monomers and  $[\text{2-}^{13}\text{C}]$ glycerol-labeled monomers, referred to as *mixed* PI3-SH3, and performed  $^{15}\text{N}$ - $^{13}\text{C}$  correlation experiments. This labeling protocol results in the random incorporation of  $^{15}\text{N}$  and  $^{13}\text{C}\alpha$  labeled monomers into the fibrils.  $[\text{2-}^{13}\text{C}]$ glycerol labeling enhances the spectral resolution and facilitates  $^{15}\text{N}$ - $^{13}\text{C}$  heteronuclear recoupling via z-filtered transferred echo double resonance (ZF-TEDOR).<sup>46</sup> In mixed PI3-SH3 samples, polarization build-up reaches a maximum at a ZF-TEDOR mixing period of  $\sim 16$  ms for  $^{13}\text{C}$  backbone sites, consistent with a  $^{15}\text{N}$ - $^{13}\text{C}$  internuclear distance of  $\sim 4.5$  Å. We recorded 2D  $^{15}\text{N}$ - $^{13}\text{C}$  correlation spectra of mixed PI3-SH3 with a mixing period of 15.36 ms, illustrated in Fig. 5(a-c). This spectrum, recorded at room temperature ( $\sim 300$  K) and a  $^1\text{H}$  frequency of 750 MHz, required a period of 16 days of signal averaging



to obtain adequate signal-to-noise. Because of the manner in which the labeling was performed, the cross peaks in the spectrum are exclusively intermolecular in origin, and therefore constrain the alignment of proteins within the fibril with respect to one another. As shown in Figure 5(g), illustrating the position of the  $\beta$ -strands determined in previous work,<sup>16</sup> we were able to assign 23  $^{15}\text{N}$ - $^{13}\text{C}\alpha$  cross-peaks in the ZF-TEDOR spectra. These assignments, based on our previously published data, are consistent with a parallel, in-register arrangement of the strands. However, we note that of the 86 residues in the sequence, we observe only about 30 cross-peaks in the aliphatic region and that the intensities of many of these are weak due to relaxation processes. In particular, protein dynamics interfere with the decoupling, recoupling and cross-polarization and lead to intensity losses in the spectra.<sup>40, 41</sup> Similar intensity losses are particularly apparent in the aromatic region of the spectrum recorded at 300 K (Figure 5(b)) that is entirely devoid of cross peaks. While twofold flips of the aromatic rings at room temperature are known to attenuate cross-polarization intensities,<sup>47</sup> the aromatic side-chains of PI3-SH3 are nevertheless present in  $^{13}\text{C}$  CP spectra. However, relaxation attenuates them during the subsequent ZF-TEDOR mixing period of 15-20 ms.

To address these intensity losses due to dynamics, we have performed low temperature (100 K) dynamic nuclear polarization (DNP) experiments at a  $^1\text{H}$  frequency of 400 MHz (263 GHz for electrons). The DNP microwave irradiation produced a signal enhancement factor of  $\sim 30$  in a mixed PI3-SH3 sample doped with the biradical polarizing agent TOTAPOL.<sup>48</sup> This enhancement factor is similar to those observed for other amyloid fibrils and nanocrystals in this experimental configuration,<sup>43</sup> and if the protein were  $^2\text{H}$  labeled, this enhancement could be a factor of  $\sim 3$ -4 larger.<sup>49</sup> A DNP-enhanced ZF-TEDOR spectrum of this sample, acquired in 32 hours and shown in Fig. 5(d-f), reveals many additional intermolecular  $^{15}\text{N}$ - $^{13}\text{C}$  cross-peaks. Note that the low temperature in this cryoprotected fibril sample induces only moderate line broadening, and the effect is fully reversible; that is, the 300 K spectrum is unchanged before and after freezing. Importantly, low temperatures improve the overall long-range polarization transfer efficiency of ZF-TEDOR because they quench the dynamic processes that lead to short relaxation times. The temperature effect is most dramatically illustrated in the  $^{13}\text{C}$  aromatic region (Fig. 5(b) vs. 5(e)) which is empty at 300 K, but is well populated with cross peaks at 100 K. Similar effects are also observed in the carbonyl (5(a) vs. 5(d)) and aliphatic (5(c) vs. 5(f)) regions of the DNP spectrum, which reveal many additional cross-peaks. Thus, the low temperatures required for DNP enhancement provide not only an additional factor of three in Boltzmann polarization, but they also improve the detection efficiency of intermolecular correlations without significantly compromising spectral resolution. To date a total of 52 intermolecular  $^{15}\text{N}$ - $^{13}\text{C}\alpha$  cross peaks have been unambiguously assigned, as illustrated in Figure 5(h).

While many more signals are observed in low-temperature DNP-enhanced spectra than in room-temperature spectra, it is also more difficult to assign peaks uniquely in the former. This is primarily due to three factors: (1) the broader lines resulting primarily from slight structural heterogeneity at low temperature, (2) also the lower external magnetic field used in our DNP experiments and (3) the fact that many additional cross peaks are present – an embarrassment of the riches ! In particular, the average  $^{13}\text{C}$  and  $^{15}\text{N}$  line widths increase from 0.5 and 1.0 ppm, respectively, at 750 MHz and 300 K to 1.0-1.5 and 2.0-3.0 ppm, respectively, at 400 MHz and 100 K. In addition, the many additional cross-peaks at low temperature (some of which may arise from interactions between  $\beta$ -sheets) lead to resonance overlap and obscure the assignment process. Therefore the 52 uniquely assigned constraints are only a fraction of the observed and potentially assignable correlations in DNP-enhanced spectra, and some of the constraints assigned at room temperature cannot be resolved at low temperature, even though the corresponding cross-peaks are likely present. Assignment of

additional constraints from DNP-enhanced spectra could be achieved with higher-dimensional and higher field DNP experiments, selectively labeled samples, and further work at low temperatures. Finally, it should be noted that spectral resolution would be compromised more severely were it not for the exclusion of radicals dispersed in the solvent matrix away from protein molecules in this and other heterogeneous system.<sup>43, 47, 50, 51</sup>

Despite limitations in resolution, the quenching of dynamic processes at low temperature results in a richer information content than at room temperature. Since PI3-SH3 does not contain highly flexible segments, CP spectra at 100 K and 300 K present similar features, and since the DNP enhancement is virtually uniform, the enhancement factor is similar for different sites in the fibril. However, the heteronuclear  $^{15}\text{N}$ - $^{13}\text{C}$  mixing period is sensitive to dynamics on a different time scale than CP experiments, and leads to depolarization at room temperature but not at 100 K. Thus while many interstrand cross-peaks are missing from ZF-TEDOR spectra at 300 K, they appear more uniformly in spectra at 100 K, as can be seen in Figure 5. In contrast, the intermolecular ZF-TEDOR signal intensities at room temperature vary drastically for different sites along the peptide chain depending on local dynamics. Finally, it is worth noting that frequently MAS spectra of proteins in membranes and fibrils are observed to exhibit reduced signal intensities when compared with spectra of microcrystalline samples such as  $\text{G}_{\text{B1}}$ . It is not uncommon that regions of the peptide chain are not present in multidimensional spectra. A large part of the reason for this behavior is undoubtedly due to dynamic processes present at ambient temperatures. Thus, proper cryoprotection of the protein samples, which permits spectra to be recorded at low temperatures, should address this problem in many cases.

As Figure 5 shows, many of the cross-peaks observed in mixed PI3-SH3 can be assigned to  $^{15}\text{N}(i)$ - $^{13}\text{C}\alpha(i)$  or  $^{15}\text{N}(i)$ - $^{13}\text{C}'(i-1)$  backbone resonance pairs in which each nucleus belongs to neighboring molecules in the fibrils. Only a parallel, in-register supramolecular architecture, in which the closest interstrand  $^{15}\text{N}$ - $^{13}\text{C}$  contacts are  $^{15}\text{N}(i)$ - $^{13}\text{C}\alpha(i)$  and  $^{15}\text{N}(i)$ - $^{13}\text{C}'(i-1)$  pairs with internuclear distances of 4.3 to 5 Å, can generate the intermolecular correlation pattern observed for *mixed* PI3-SH3. Therefore, the *mixed* PI3-SH3 data corroborate the conclusions obtained through the analysis of long-range  $^{13}\text{C}$ - $^{13}\text{C}$  correlation spectra of 2-PI3-SH3 described in the previous sections and provide additional structural constraints. A graphical summary of all of the constraints obtained from both the  $^{13}\text{C}$ - $^{13}\text{C}$  and  $^{15}\text{N}$ - $^{13}\text{C}$  experiments is shown in Fig. 6(a). In particular, we note that combining homonuclear experiments with heteronuclear MAS NMR experiments on mixed samples and with DNP enhancement yields a total of 111 intermolecular constraints spanning the length of the peptide chain.

### Refined model for PI3-SH3 amyloid protofilament

In a previous publication we reported the chemical shift assignments for PI3-SH3 amyloid fibrils and were able to establish the position of the  $\beta$ -strands in the protein in its fibrillar form via a TALOS analysis of the shifts.<sup>16</sup> In particular, we found the protein to contain four  $\beta$ -strands regions which could be divided approximately into two segments each of  $\sim 40$  Å length (see Figure 5(g) and (h)). Furthermore, we assumed that these two segments are folded in the middle, and showed that they then fit into the cross section of the electron density profile published by Jimenez, et al.<sup>52</sup> This was illustrated in Figure 8 of our previous publication.<sup>16</sup> At the time we described this model, we suggested that the  $\beta$ -strands were arranged in a parallel, in-register configuration, but this proposal was based solely on the fact that the length of the strands was consistent with the dimensions of the cross section of the fibril determined by cryoEM where peaks in the electron density profile are observed with a  $\sim 40$  Å separation. The interstrand experiments reported here confirm the parallel in-register hypothesis, and therefore represent a refinement of this model as shown in Figure 6b. We have included in this illustration the interstrand  $^{15}\text{N}$ - $^{13}\text{C}\alpha$  contacts derived from the

spectra in Figure 5 and summarized graphically in Figure 6a. The position of the turn between  $\beta$ -sheets is consistent with chemical shift analysis and the dimensions of the fibril cross-section; however the detailed structure of this model of intramolecular interface of the  $\beta$ -sheets requires additional experimental verification and refinement.

## Conclusions

We have described three spectroscopic methods able to identify the presence of a parallel, in-register  $\beta$ -sheet tertiary structure in amyloid fibrils, and have shown their applicability in a study of fibrils derived from PI3-SH3. First, using samples prepared with 2- $^{13}\text{C}$  glycerol labeling, we detected  $^{13}\text{C}\alpha$ - $^{13}\text{C}\alpha$  contacts between adjacent  $\beta$ -strands and between neighboring molecules using the efficient BASE RFDR recoupling sequence. This approach was used to elucidate regions of high structural degeneracy in amyloid fibrils, which are consistent with a parallel, in-register intermolecular organization. In a second and complementary approach, comparison of short-range and long-range  $^{13}\text{C}$ - $^{13}\text{C}$  correlations enabled the differentiation between intra- and inter-residue contacts due to mutually exclusive  $^{13}\text{C}$ - $^{12}\text{C}$  and  $^{12}\text{C}$ - $^{13}\text{C}$  pairs. Such pairs are often present in molecules produced with [2- $^{13}\text{C}$ ] glycerol labeling and allowed the direct observation of correlations between the strands forming parallel, in-register  $\beta$ -sheets in PI3-SH3 amyloid fibrils. The major advantage of these homonuclear strategies is that they rely on the analysis of robust experiments that can be recorded efficiently, and on labeling schemes commonly used in structure determination efforts. As a third, more general approach, we have shown that low-temperature DNP-enhanced heteronuclear correlation spectroscopy of a mixed  $^{15}\text{N}/^{13}\text{C}$  sample provides a large number of highly sensitive supramolecular constraints. Low-temperature DNP-enhanced spectroscopy thus constitutes the most powerful and possibly widely applicable approach for the structural characterization of intricate molecular assemblies such as amyloid fibrils and their oligomeric intermediates. It provides unprecedented enhancements in signal-to-noise and the low temperatures quench the dynamics that otherwise would attenuate structurally important cross-peak intensities. This approach should be also widely applicable to studies of protein-protein interactions and limited only by the resolution available in the multidimensional spectra. It offers a solution to the observation of “missing resonances” frequently observed in MAS spectra of proteins in membranes and fibrils.

## Materials and Methods

### Protein samples

A sample of the  $\beta_1$  domain of immunoglobulin protein G ( $G_{\beta_1}$ , 56 residues) in microcrystalline form was prepared using [2- $^{13}\text{C}$ ]glycerol and  $^{13}\text{C}$  bicarbonate as the sole sources of carbon and uniform  $^{15}\text{N}$  labeling (2- $G_{\beta_1}$ ). Production, purification and crystallization of  $G_{\beta_1}$  were carried out following previously published protocols,<sup>53</sup> the precipitation step being performed so as to yield microcrystals in trigonal form.<sup>53</sup> Approximately 20 mg of protein were packed in a 3.2 mm rotor. For homonuclear studies, two types of PI3-SH3 amyloid fibril samples were used, one labeled uniformly with [U- $^{13}\text{C}$ ]glucose (U-PI3-SH3) and the other prepared with [2- $^{13}\text{C}$ ]glycerol and  $\text{NaH}^{13}\text{CO}_3$  as the sources of carbon (2-PI3-SH3), while both were uniformly  $^{15}\text{N}$  labeled with  $^{15}\text{NH}_4\text{Cl}$ . For the mixed  $^{15}\text{N}/^{13}\text{C}$  PI3-SH3 sample, the  $^{15}\text{N}$  component was prepared with  $^{15}\text{NH}_4\text{Cl}$  and glucose at natural abundance, while the  $^{13}\text{C}$  component was prepared with [2- $^{13}\text{C}$ ]glycerol and  $\text{NaH}^{13}\text{CO}_3$  as the sources of carbon. The fibrils were grown from a solution of monomeric protein by incubation at pH 2.0 and 25 °C for a period of 14 days as described previously,<sup>30</sup> resulting in the generation of a gel-like solution containing fibrils that were subsequently centrifuged and dispersed in a  $d_5$ -glycerol/water solvent (60/40, w/w) to cryoprotect the samples. For the DNP experiments, TOTAPOL biradicals were added



to the glycerol/water solvent at a concentration of 10 mM (20 mM electrons). After a final centrifugation step, approximately 8 mg aliquots of fibrils were packed into 3.2 mm rotors.

### MAS NMR spectroscopy

Homonuclear correlation experiments were performed in a spectrometer operating at 700 MHz  $^1\text{H}$  frequency (courtesy of Dr. David J. Ruben, Francis Bitter Magnet Laboratory, Cambridge MA), corresponding to a 16.4 T magnetic field, using a triple resonance Varian/Chemagnetics (Palo Alto, CA) magic-angle spinning probe equipped with a 3.2 mm stator. Sample temperatures were maintained at 5 °C with a stream of  $\text{N}_2$  gas cooled. All experiments were acquired using  $^1\text{H}$ - $^{13}\text{C}$  cross-polarization and TPPM  $^1\text{H}$  decoupling<sup>54</sup> was applied during the chemical shift evolution and detection periods. Two-dimensional BASE RFDR<sup>36</sup> experiments consisted of 544 total t1 points acquired in 60  $\mu\text{s}$  increments with a 3.0 s recycle delay and were recorded with a mixing time  $\tau_{\text{mix}} = 24$  ms, 12.5 kHz  $^{13}\text{C}$   $\pi$  pulses, and 80 kHz  $^1\text{H}$  decoupling, at a spinning frequency  $\omega_r/2\pi = 12.5$  kHz, with a 32-step phase sequence in the low-power  $^{13}\text{C}$  pulses described previously.<sup>36</sup> The total acquisition times were 7.5 hours for 2- $\text{G}_{\text{B1}}$  and 120 hours for 2-PI3-SH3, corresponding to 16 and 256 scans per t1 point, respectively. Similar acquisition parameters were used to record PDS spectra, with 16 scans per t1 point for the U-PI3-SH3 spectrum and 192 scans per t1 point for each 2-PI3-SH3 spectrum (with short and long mixing periods). Spectra were analyzed with the Sparky program (T.D. Goddard and D.G. Kneller, SPARKY 3.115, University of California, San Francisco).

The room temperature ZF-TEDOR experiment was acquired on a 750 MHz spectrometer equipped with a 3.2 mm triple resonance  $^1\text{H}/^{13}\text{C}/^{15}\text{N}$  Bruker E<sup>free</sup> probe (Billerica, MA). The sample temperature during spinning ( $\omega_r/2\pi = 12.5$  kHz) and pulsing was estimated to be  $\sim 300$  K. This 2D spectrum was acquired with 2880 scans per t1 point, 160 total t1 points, and a dwell time of 80  $\mu\text{s}$ , with a total acquisition time of 16 days. TPPM decoupling (95 kHz) was used during mixing, evolution and detection periods.

### DNP experiments

DNP-enhanced ZF-TEDOR experiments were performed on a Bruker spectrometer, operating at a  $^1\text{H}$  frequency of 400 MHz, equipped with a 263 GHz gyrotron source, a microwave transmission line, and a 3.2 mm low-temperature MAS probe (Bruker BioSpin, Billerica, MA).<sup>55</sup> The temperature was regulated at 100 K, and the spinning frequency was set to 9 kHz. A 2.5  $\mu\text{s}$   $^1\text{H}$  pulse followed by a 800  $\mu\text{s}$  spin-lock pulse were used for  $^{13}\text{C}$  cross-polarization, while 4.5  $\mu\text{s}$   $^{13}\text{C}$   $\pi/2$  pulses, and 6.25  $\mu\text{s}$   $^{15}\text{N}$   $\pi/2$  pulses were used during the mixing period. TPPM  $^1\text{H}$  decoupling (100 kHz) was used during mixing, evolution, and detection periods. A series of six 2D experiments were averaged together, each of which was recorded with 32 scans per t1 point, 160 total t1 points, 111  $\mu\text{s}$  indirect dwell time, and a recycle delay of 3.8 sec ( $\sim 5.4$  hr per experiment).

### Acknowledgments

We thank our colleagues L. Andreas, A.B. Barnes, B. Corzilius, E. Daviso, K. Frederick, V. Michaelis, E. Markhasin, Qing Ni, T.C. Ong, M. Reese, A.A. Smith, D.J. Ruben, and C.J. Turner for their assistance and stimulating conversations during the course of this research. This research was supported by the National Institutes of Health through grants EB-003151, EB-002804 and EB-002026 and by the Wellcome Trust.

### References

1. Sunde M, Serpell LC, Bartlam M, Fraser PE, Pepys MB, Blake CC. *J Mol Biol.* 1997; 273(3):729–739. [PubMed: 9356260]
2. Sunde M, Blake CC. *Q Rev Biophys.* 1998; 31(1):1–39. [PubMed: 9717197]

3. Dobson CM. *Nature*. 2003; 426(6968):884–890. [PubMed: 14685248]
4. Chiti F, Dobson CM. *Annu Rev Biochem*. 2006; 75:333–366. [PubMed: 16756495]
5. Fowler DM, Koulov AV, Balch WE, Kelly JW. *Trends in Biochemical Sciences*. 2007; 32:217–224. [PubMed: 17412596]
6. Dobson CM. *Trends in Biochemical Sciences*. 1999; 24:329–332. [PubMed: 10470028]
7. Knowles TP, Fitzpatrick AW, Meehan S, Mott HR, Vendruscolo M, Dobson CM, Welland ME. *Science*. 2007; 318(5858):1900–1903. [PubMed: 18096801]
8. Benzinger TL, Gregory DM, Burkoth TS, Miller-Auer H, Lynn DG, Botto RE, Meredith SC. *Proc Natl Acad Sci USA*. 1998; 95(23):13407–13412. [PubMed: 9811813]
9. Antzutkin ON, Leapman RD, Balbach JJ, Tycko R. *Biochemistry*. 2002; 41(51):15436–15450. [PubMed: 12484785]
10. Jaroniec CP, MacPhee CE, Astrof NS, Dobson CM, Griffin RG. *Proc Natl Acad Sci USA*. 2002; 99(26):16748–16753. [PubMed: 12481032]
11. Heise H, Hoyer W, Becker S, Andronesi OC, Riedel D, Baldus M. *Proc Natl Acad Sci USA*. 2005; 102(44):15871–15876. [PubMed: 16247008]
12. Ritter C, Maddelein ML, Siemer AB, Lührs T, Ernst M, Meier BH, Saupe SJ, Riek R. *Nature*. 2005; 435(7043):844–848. [PubMed: 15944710]
13. Helmus JJ, Surewicz K, Nadaud PS, Surewicz WK, Jaroniec CP. *Proc Natl Acad Sci USA*. 2008; 105(17):6284–6289. [PubMed: 18436646]
14. Andronesi OC, von Bergen M, Biernat J, Seidel K, Griesinger C, Mandelkow E, Baldus M. *J Am Chem Soc*. 2008; 130(18):5922–5928. [PubMed: 18386894]
15. Debelouchina GT, Platt GW, Bayro MJ, Radford SE, Griffin RG. *J Am Chem Soc*. 2010; 132(30):10414–10423. [PubMed: 20662519]
16. Bayro MJ, Maly T, Birkett NR, MacPhee CE, Dobson CM, Griffin RG. *Biochemistry*. 2010; 49(35):7474–7484. [PubMed: 20707313]
17. Jaroniec CP, MacPhee CE, Bajaj VS, McMahon MT, Dobson CM, Griffin RG. *Proc Natl Acad Sci USA*. 2004; 101(3):711–716. [PubMed: 14715898]
18. Petkova AT, Yau WM, Tycko R. *Biochemistry*. 2006; 45(2):498–512. [PubMed: 16401079]
19. Iwata K, Fujiwara T, Matsuki Y, Akutsu H, Takahashi S, Naiki H, Goto Y. *Proc Natl Acad Sci USA*. 2006; 103(48):18119–18124. [PubMed: 17108084]
20. Shewmaker F, Ross ED, Tycko R, Wickner RB. *Biochemistry*. 2008; 47(13):4000–4007. [PubMed: 18324784]
21. Wickner RB, Dyda F, Tycko R. *Proc Natl Acad Sci USA*. 2008; 105(7):2403–2408. [PubMed: 18268327]
22. Wasmer C, Lange A, Van Melckebeke H, Siemer AB, Riek R, Meier BH. *Science*. 2008; 319(5869):1523–1526. [PubMed: 18339938]
23. Antzutkin ON, Balbach JJ, Leapman RD, Rizzo NW, Reed J, Tycko R. *Proc Natl Acad Sci USA*. 2000; 97(24):13045–13050. [PubMed: 11069287]
24. Balbach JJ, Petkova AT, Oyler NA, Antzutkin ON, Gordon DJ, Meredith SC, Tycko R. *Biophys J*. 2002; 83(2):1205–1216. [PubMed: 12124300]
25. Petkova AT, Leapman RD, Guo Z, Yau WM, Mattson MP, Tycko R. *Science*. 2005; 307(5707):262–265. [PubMed: 15653506]
26. Lim KH, Nguyen TN, Damo SM, Mazur T, Ball HL, Prusiner SB, Pines A, Wemmer DE. *Solid State Nucl Mag*. 2006; 29(1-3):183–190.
27. Caporini M, Bajaj V, Veshtort M, Fitzpatrick A, Cait EM, Vendruscolo M, Dobson CM, Griffin RG. *J Phys Chem B*. 2010; 114:13555–13561. [PubMed: 20925357]
28. Nieuwkoop AJ, Wylie BJ, Franks WT, Shah GJ, Rienstra CM. *J Chem Phys*. 2009; 131(9):095101. [PubMed: 19739873]
29. Debelouchina GT, Platt GW, Bayro MJ, Radford SE, Griffin RG. *J Am Chem Soc*. 2010; 132:17077–17079.
30. Guijarro JI, Sunde M, Jones JA, Campbell ID, Dobson CM. *Proc Natl Acad Sci USA*. 1998; 95:4224–4228. [PubMed: 9539718]

31. Ventura S, Zurdo J, Narayanan S, Parreño M, Mangues R, Reif B, Chiti F, Giannoni E, Dobson CM, Aviles FX, Serrano L. *Proc Natl Acad Sci USA*. 2004; 101(19):7258–7263. [PubMed: 15123800]
32. Carulla N, Caddy GL, Hall DR, Zurdo J, Gairi M, Feliz M, Giralt E, Robinson CV, Dobson CM. *Nature*. 2005; 436(7050):554–558. [PubMed: 16049488]
33. Carulla N, Zhou M, Arimon M, Gairi M, Giralt E, Robinson CV, Dobson CM. *Proc Natl Acad Sci USA*. 2009; 106(19):7828–7833. [PubMed: 19416886]
34. LeMaster DM, Kushlan DM. *J Am Chem Soc*. 1996; 118:9255–9264.
35. Castellani F, van Rossum B, Diehl A, Schubert M, Rehbein K, Oschkinat H. *Nature*. 2002; 420(6911):98–102. [PubMed: 12422222]
36. Bayro MJ, Maly T, Birkett NR, Dobson CM, Griffin RG. *Angew Chem Int Ed*. 2009; 48(31): 5708–5710.
37. Bennett AE, Rienstra CM, Griffiths JM, Zhen W, Lansbury J, Griffin RG. *J Chem Phys*. 1998; 108(22):9463–9479.
38. Tycko R. *J Chem Phys*. 2007; 126(6):064506. [PubMed: 17313228]
39. Bayro MJ, Huber M, Ramachandran R, Davenport TC, Meier BH, Ernst M, Griffin RG. *J Chem Phys*. 2009; 130(11):114506. [PubMed: 19317544]
40. Long JR, Sun BQ, Bowen A, Griffin RG. *J Am Chem Soc*. 1994; 116(26):11950–11956.
41. Maus DC, Copie V, Sun BQ, Griffiths JM, Griffin RG, Luo SF, Schrock RR, Liu AH, Seidel SW, Davis WM, Grohmann A. *J Am Chem Soc*. 1996; 118(24):5665–5671.
42. Schneider R, Seidel K, Etkorn M, Lange A, Becker S, Baldus M. *J Am Chem Soc*. 2010; 132(1): 223–233. [PubMed: 20000710]
43. Debelouchina GT, Bayro MJ, vd Wel PCA, Caporini MA, Barnes AB, Rosay M, Maas WE, Griffin RG. *Phys Chem Chem Phys*. 2010; 12(22):5911–5919. [PubMed: 20454733]
44. Szeverenyi NM, Sullivan MJ, Maciel GE. *J Magn Reson*. 1982; 47:462–475.
45. Loquet A, Giller K, Becker S, Lange A. *Jour Amer Chem Soc*. 2010; 132:15164–1516. [PubMed: 20932028]
46. Jaroniec C, Filip C, Griffin R. *J Am Chem Soc*. 2002; 124(36):10728–10742. [PubMed: 12207528]
47. Bajaj VS, vd Wel PCA, Griffin RG. *Jour Amer Chem Soc*. 2009; 131:118–128. [PubMed: 19067520]
48. Song C, Hu KN, Joo CG, Swager TM, Griffin RG. *J Am Chem Soc*. 2006; 128:11385–90. [PubMed: 16939261]
49. Akbey Ü, Franks WT, Linden A, Lange S, Griffin RG, Rossum BJv, Oschkinat H. *Angewandte Chemie International Edition*. 2010; 49:7803–7806.
50. van der Wel PCA, Hu KN, Lewandowski J, Griffin RG. *J Am Chem Soc*. 2006; 128(33):10840–10846. [PubMed: 16910679]
51. Mak-Jurkauskas ML, Bajaj VS, Hornstein MK, Belenky M, Griffin RG, Herzfeld J. *Proc Nat'l Acad Sci*. 2008; 105:883–888. [PubMed: 18195364]
52. Jimenez J, Guijarro JI, Orlova E, Zurdo J, Dobson CM, Sunde M, Saibil HR. *The EMNO Journal*. 1999; 18(4):815–821.
53. Frericks Schmidt HL, Sperling LJ, Gao YG, Wylie BJ, Boettcher JM, Wilson SR, Rienstra CM. *J Phys Chem B*. 2007; 111(51):14362–14369. [PubMed: 18052145]
54. Bennett AE, Rienstra CM, Auger M, Lakshmi KV, Griffin RG. *J Chem Phys*. 1995; 103(16):6951–6958.
55. Debelouchina GT, Bayro MJ, vd Wel PCA, Caporini MA, Barnes AB, Rosay M, Maas WE, Griffin RG. *Phys Chem Chem Phys*. 2010; 12

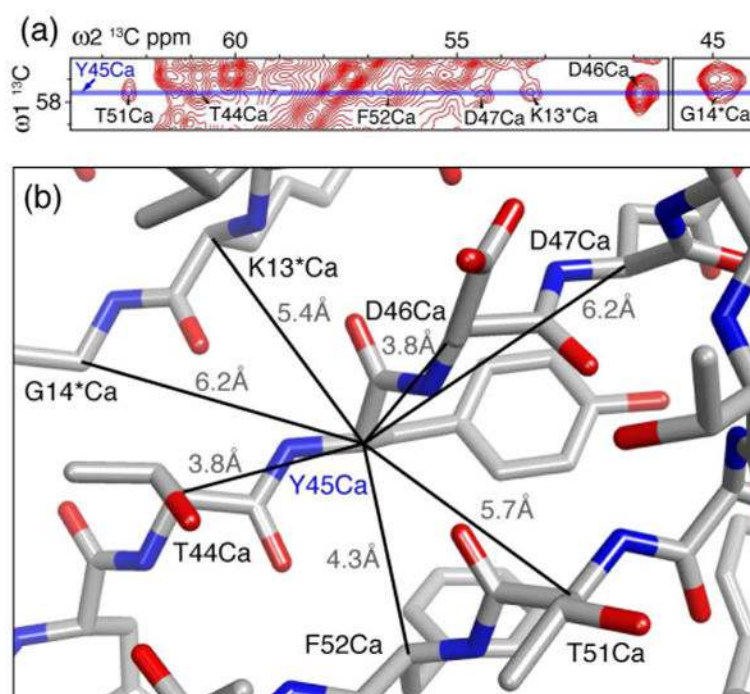


**Figure 1.**

(a) Sub-section of a BASE RFDR spectrum of microcrystalline 2- $G_{B1}$  showing cross-peaks between Y45Ca and neighboring nuclei. (b) Inter-nuclear distances in the crystal structure of  $G_{B1}$  (PDB ID 2QMT) corresponding to the cross-peaks observed between Y45Ca and other  $^{13}\text{C}$  sites, i.e., within its own strand (T44, D46, and D47), to a strand within the same molecule (T51 and F52), and to an adjacent strand in a neighboring molecule (K13\* and G14\*). Asterisks denote residues in an adjacent protein molecule in the crystal lattice. The spectrum in (a) was recorded with  $\tau_{\text{mix}} = 24$  ms and a total experimental time of 7.5 hours.

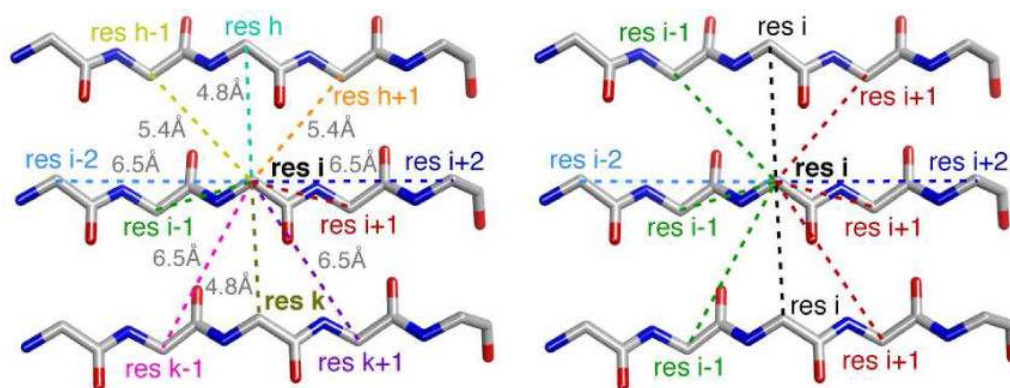


**Figure 2.**

Inter-nuclear distances anticipated in parallel  $\beta$ -strands and resolvable  $^{13}\text{C}_\alpha$ - $^{13}\text{C}_\alpha$  correlations for a given residue in the middle of three different strands  $h$ ,  $i$ ,  $k$  (left), and three identical in-register strands  $i$ ,  $i$ ,  $i$  (right). Inter-strand correlations in the parallel in-register case are degenerate with sequential correlations within the strand. Typical internuclear distances are indicated on the left. Dashed lines of different colors (except for black) indicate the potentially resolved cross-peaks in  $^{13}\text{C}$ - $^{13}\text{C}$  correlation spectra.



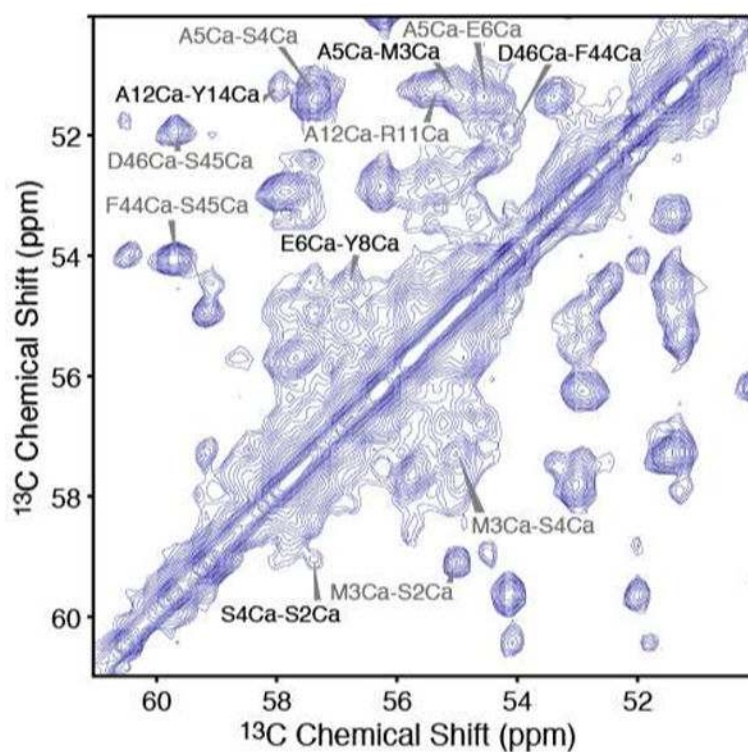


**Figure 3.** Section of a BASE RFDR spectrum of amyloid fibrils formed by 2-PI3-SH3. Gray labels indicate sequential  $^{13}\text{C}\alpha$ - $^{13}\text{C}\alpha$  cross-peaks while black labels denote cross-peaks between  $^{13}\text{C}\alpha$  nuclei separated by two residues, with an inter-nuclear distance corresponding to  $\sim 6.5$  Å. Backbone-backbone correlations between sites distant in space, but near in sequence, are readily observed for several regions of the polypeptide chain. This spectrum was recorded with  $\tau_{\text{mix}} = 24$  ms and a total experimental time of 5 days.

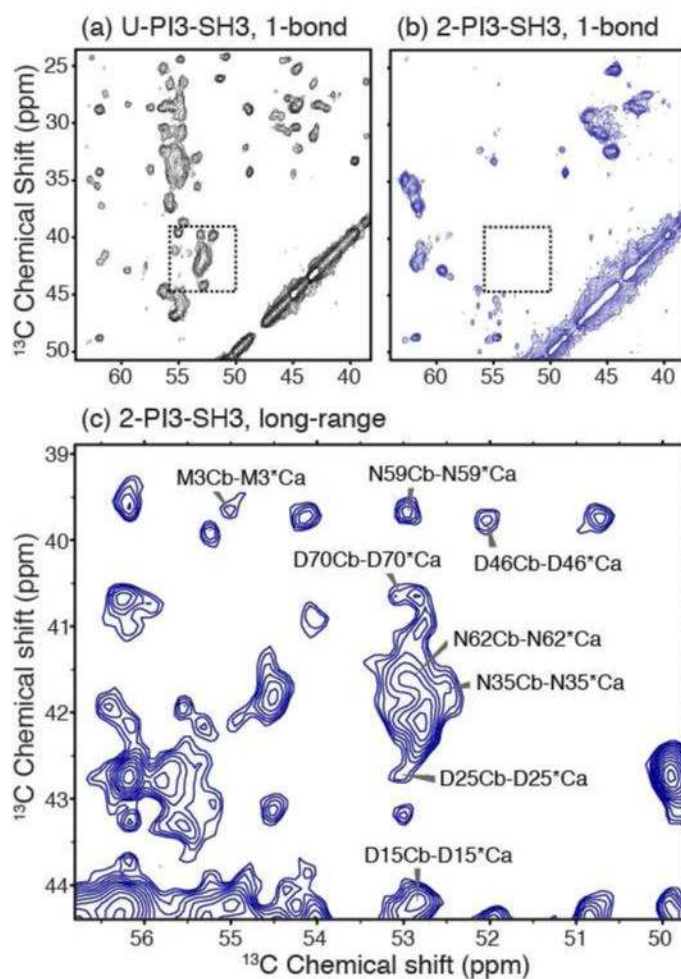


**Figure 4.** Sections of PDS  $^{13}\text{C}$ - $^{13}\text{C}$  correlation spectra acquired with a mixing time of 20 ms optimized for one-bond correlations of (a) U-PI3-SH3 and (b) 2-PI3-SH3, and with a mixing time of 500 ms optimized for long-range correlations in (c) 2-PI3-SH3. The dotted boxes in (a) and (b) correspond to the same region as that shown in (c), in which asterisks identify correlations between neighboring molecules in a parallel, in-register architecture.

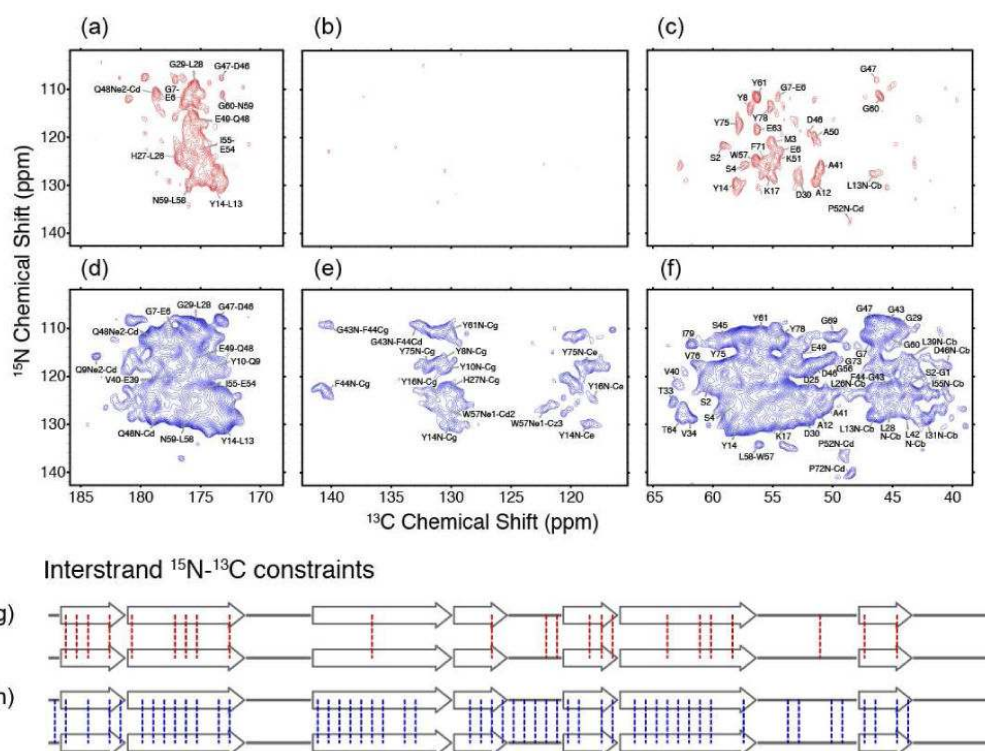


**Figure 5.** (a-c) 750 MHz intermolecular  $^{15}\text{N}$ - $^{13}\text{C}$  correlations in PI3-SH3 fibrils recorded at 300 K with 16 days of acquisition. The three panels correspond to the  $^{15}\text{N}$ - $^{13}\text{C}=\text{O}$ , aromatic, and  $^{15}\text{N}$ - $^{13}\text{C}\alpha$  regions of the spectra. (d-f) The identical spectral regions recorded at 100 K and 400 MHz with DNP enhancement in 32 hours of signal averaging. The spectra were obtained with ZF-TEDOR recoupling ( $\tau_{\text{mix}} = 16$  ms) from a mixed PI3-SH3, a sample fibrillized from a mixture of  $[\text{15N}]$  monomers and  $[\text{2-13C}]$  monomers. (g) Illustration of the 23 interstrand contacts established from  $^{13}\text{C}$ - $^{15}\text{N}$  cross peaks in the 750 MHz spectra acquired at 300 K in (a-c); (h) the 52 interstrand contacts established from the 400 MHz DNP enhanced spectra recorded at 100 K shown in (d-f).

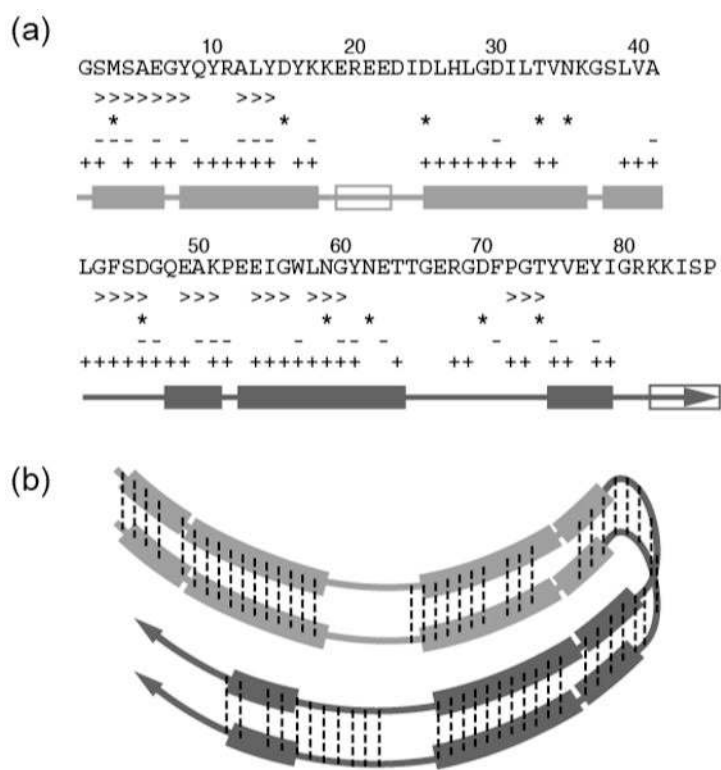


**Figure 6.**

(a) Summary of intermolecular constraints along the PI3-SH3 sequence obtained with the methods described in the text: Indirect CC (“>”), direct CC (“\*”), mixed NC at room temperature (“-“), and mixed NC at 100 K with DNP (“+”). Filled bars indicate residues in a  $\beta$ -strand conformation while empty bars mark dynamic regions that have not been assigned in the spectra. (b) Superposition of all intermolecular constraints on a hypothetical model of PI3-SH3 amyloid fibril architecture in which two  $\beta$ -sheet layers (light gray and dark gray, respectively) are formed by each half of the sequence.